

Critical Thresholds for Deep ${\rm CO}_2$ Foam Generation Effects of Injected Quality, Surfactant Concentration and Permeability

Wei, B.; Yang, M.; Tang, J.; Wang, Y.; Lu, J.; Rossen, W. R.

10.2118/218255-MS

Publication date

Document Version Final published version

Published in

Society of Petroleum Engineers - SPE Improved Oil Recovery Conference, IOR 2024

Citation (APA)
Wei, B., Yang, M., Tang, J., Wang, Y., Lu, J., & Rossen, W. R. (2024). Critical Thresholds for Deep CO
Foam Generation: Effects of Injected Quality, Surfactant Concentration and Permeability. In *Society of* Petroleum Engineers - SPE Improved Oil Recovery Conference, IOR 2024 Article SPE-218255-MS
(Proceedings - SPE Symposium on Improved Oil Recovery; Vol. 2024-April). Society of Petroleum Engineers (SPE). https://doi.org/10.2118/218255-MS

To cite this publication, please use the final published version (if applicable). Please check the document version above.

Copyright

Other than for strictly personal use, it is not permitted to download, forward or distribute the text or part of it, without the consent of the author(s) and/or copyright holder(s), unless the work is under an open content license such as Creative Commons.

Please contact us and provide details if you believe this document breaches copyrights. We will remove access to the work immediately and investigate your claim.

Green Open Access added to TU Delft Institutional Repository 'You share, we take care!' - Taverne project

https://www.openaccess.nl/en/you-share-we-take-care

Otherwise as indicated in the copyright section: the publisher is the copyright holder of this work and the author uses the Dutch legislation to make this work public.



Critical Thresholds for Deep CO₂ Foam Generation: Effects of Injected Quality, Surfactant Concentration and Permeability

B. Wei and M. Yang, State Key Laboratory of Oil and Gas Reservoir Geology and Exploitation, Southwest Petroleum University; J. Tang, Department of Chemical and Petroleum Engineering, United Arab Emirates University; Y. Wang and J. Lu, McDougall School of Petroleum Engineering, The University of Tulsa; W. R. Rossen, Department of Geoscience and Engineering, Delft University of Technology

Copyright 2024, Society of Petroleum Engineers DOI 10.2118/218255-MS

This paper was prepared for presentation at the SPE Improved Oil Recovery Conference held in Tulsa, Oklahoma, USA, 22 - 25 April 2024.

This paper was selected for presentation by an SPE program committee following review of information contained in an abstract submitted by the author(s). Contents of the paper have not been reviewed by the Society of Petroleum Engineers and are subject to correction by the author(s). The material does not necessarily reflect any position of the Society of Petroleum Engineers, its officers, or members. Electronic reproduction, distribution, or storage of any part of this paper without the written consent of the Society of Petroleum Engineers is prohibited. Permission to reproduce in print is restricted to an abstract of not more than 300 words; illustrations may not be copied. The abstract must contain conspicuous acknowledgment of SPE copyright.

Abstract

Long-distance propagation of foam is one key to deep gas mobility control for enhanced oil recovery and CO_2 sequestration. It depends on two processes: convection of bubbles and foam generation at the displacement front. Prior studies with N_2 foam show the existence of a critical threshold for foam generation in terms of a minimum pressure gradient (∇p_{gen}^{min}) or minimum total interstitial velocity $(v_{t,gen}^{min})$, beyond which strong-foam generation is triggered. The same mechanism controls foam propagation. There are few data for ∇p_{gen}^{min} or $v_{t,gen}^{min}$ for CO_2 foam.

We extend previous studies to quantify ∇p_{gen}^{min} and $v_{t,gen}^{min}$ for CO_2 foam generation, and relate ∇p_{gen}^{min} and $v_{t,gen}^{min}$ with factors including injected quality (gas volume fraction in the fluids injected) - f_g , surfactant concentration - C_s , and permeability - K. In each experiment, steady pressure gradient, ∇p , is measured at fixed injection rate and quality, with total interstitial velocity, v_t , increasing-then-decreasing in a series of steps. The trigger for strong-foam generation features an abrupt jump in ∇p upon an increase in v_t .

In most cases, the data for ∇p as a function of v_t identify three regimes: coarse foam with low ∇p , an abrupt jump in ∇p , and strong foam with high ∇p . The abrupt jump in ∇p upon foam generation demonstrates the existence of ∇p_{gen}^{min} and $v_{t,gen}^{min}$ for CO_2 foam. We further show how ∇p_{gen}^{min} and $v_{t,gen}^{min}$ scale with f_g , C_s and K. Conditions that stabilize lamellae reduce the values of the thresholds: both ∇p_{gen}^{min} and $v_{t,gen}^{min}$ increase with f_g and decrease with increasing C_s or K. Specifically, ∇p_{gen}^{min} scales with f_g as $(f_g)^2$ and $v_{t,gen}^{min}$ scales as $(f_g)^4$, and both ∇p_{gen}^{min} and $v_{t,gen}^{min}$ scale with C_s as $(C_s)^{-0.4}$. The effect of K on the thresholds for foam generation is greater than the effects of f_g and G_s . Our data in artificial consolidated cores show that ∇p_{gen}^{min} scales with K as K^{-2} for CO_2 foam, in comparison to K^{-1} for N_2 foam in unconsolidated sand/bead packs. More data are needed to verify the confidence of these correlations.

It is encouraging that ∇p_{gen}^{min} in the cores with K=270 mD or greater is less than 0.17 bar/m (~ 0.75 psi/ft), 2 to 3 orders of magnitude less than for N₂ foam. Such low ∇p_{gen}^{min} can be easily attainable throughout a formation. This suggests that: limited ∇p deep in formations is much less of a restriction for long-distance propagation of CO_2 foam than for N₂ foam. Foam propagation could still be challenging in low-K reservoirs ($\nabla p_{gen}^{min} \sim 10$ bar/m for K=27 mD). Nevertheless, formation heterogeneity and alternating slug injection of gas and liquid help foam generation and may well reduce the values of ∇p_{gen}^{min} . More research is needed to predict long-distance propagation of foam under those conditions.

Introduction

Gas injection into geological formations is often subject to very poor volumetric sweep efficiency (Rossen, 1996). This results from issues including gravity segregation (due to lower gas density than liquids), gas fingering (due to greater gas mobility than liquids) and channeling (due to formation heterogeneity). Foam is currently the most effective means for gas sweep improvement, given that it can reduce gas mobility considerably, e.g. by a factor $10 - 10^4$. This unique feature allows foam to have a variety of applications in subsurface processes, e.g., enhanced oil recovery (EOR), acid diversion in well stimulation and soil/aquifer remediation. Foam can also be a promising means for carbon capture and storage (CCS), beneficial to both improved sweep and safe trapping of CO_2 in place (Rognmo et al., 2018; Rossen et al., 2022).

Foam can be easily created in the vicinity of an injection well, where pressure gradient and velocity are high. Nevertheless, to improve mobility ratio deep into the formation, foam must propagate a long distance at low pressure-gradient and low superficial velocity. Many studies address foam stability and propagation in porous rocks, based on measurements of half-life time of bulk foam in column tests (e.g., AlYousef et al., 2018; Bello et al., 2022; Yu et al., 2023). However, the mechanisms between the two cases are different. Foam stability in bulk is governed by drainage of liquid over the height of the column, and therefore sensitive to liquid viscosity, but a function of local capillary pressure in porous media (Khatib et al., 1988; Rossen and Zhou, 1995; Alvarez et al., 2001). In addition, foam texture (bubble size) is very different in the two cases. Individual bubble size in bulk is much smaller than container in foam column tests but is about or greater than pore size in porous rocks; thus diffusion plays a different role in foam stability. Thus, one cannot extrapolate half-life time in column tests to foam behavior in porous rocks, though the column test is a good means for quick screening of foaming agents.

In geological formations, long-distance propagation of foam is driven by two simultaneous processes: convections of bubbles and generation at the displacement front. One key issue concerns the conditions for delivering foam deep in a formation. where pressure gradient and superficial velocity are low. Reported data for N_2 foam show a minimum pressure gradient (∇p_{gen}^{min}) or minimum total interstitial velocity ($v_{t,gen}^{min}$) beyond which foam generation is allowed (Gauglitz et al., 2002). The minimum velocity and pressure gradient for foam propagation depend on similar mechanisms, though the pressure gradient for propagation is greater, and the velocity less, than that for generation (Yu et al.2020). In many cases, observed values of ∇p_{gen}^{min} or $v_{t,gen}^{min}$ in the laboratory for N_2 foam (Yu et al., 2020) are way too high to be seen in the field. This suggests that long-distance propagation of N_2 foam could be challenging. However, there are few data available in the literature for CO_2 foam (Gauglitz et al., 2002). One may expect lower ∇p_{gen}^{min} or $v_{t,gen}^{min}$ for CO_2 foam as surface tension for supercritical CO_2 -water is lower than N_2 -water. Nevertheless, the quantitative conditions for CO_2 -foam generation and propagation are unclear: in particular, under low pressure gradient/velocity conditions away from an injection well.

The goal of the study is to quantify the ∇p_{gen}^{min} and $v_{t,gen}^{min}$ required for CO_2 foam generation in porous media. Furthermore, we correlate ∇p_{gen}^{min} and $v_{t,gen}^{min}$ with crucial factors, including injected foam quality (volumetric

gas fraction in foam, f_g), surfactant concentration (C_s) and medium permeability (K). Other factors, such as heterogeneity and alternate injection of gas and liquid, also help foam generation. For this study, we examine steady gas-liquid injection through homogeneous, artificial consolidated cores. The measured data for ∇p_{gen}^{min} and $v_{t,gen}^{min}$ reveal the mechanisms and triggering conditions for CO_2 foam generation. The results would be a valuable reference to evaluate the feasibility or optimize the projects requiring deep CO_2 propagation in the field. Furthermore, the data could be used to fit the model parameters for field-scale simulation of foaminjection processes.

Brief Review on Foam Generation in Porous Media

The generation of foam is a process of creation and accumulation of lamellae, i.e. thin liquid films separating bubbles (Rossen and Gauglitz, 1990). Thus, foam generation is related to lamella creation but not identical. It requires lamella creation rate be greater than destruction rate. This means that the stability of lamellae is crucial, given that many factors may destabilize foam, e.g. most oils (Farajzadeh et al., 2012; Tang et al., 2019a; Tang et al., 2019b).

Mechanisms of Lamella Creation

Four mechanisms have been identified for lamella creation (Ransohoff and Radke, 1988; Rossen, 1996; 2003): (1) "leave behind" that creates lamellae via gas invasion into a medium initially saturated with water; (2) "snap-off" that creates lamellae in pore throats, where water films bridge throats at sufficiently low capillary pressure; (3) "lamella division" that creates new lamellae when a lamella is forced through a pore body connected to several pore throats. Lamella division requires a sufficient pressure gradient to mobilize the lamella through pore throats. (4) "gas evolution within liquid" that creates foam when gas is generated in surfactant solution.

Foam Generation at Fixed Quality

After a period of steady gas/liquid injection, creation of foam at the same quality depends on injection rate and pressure gradient. The generation of strong foam, with large mobility reduction, from a state of "coarse" foam, with little or no mobility reduction, features an abrupt, large increase in pressure gradient (∇p) and apparent viscosity (μ_{app} , i.e. the inverse of total relative mobility of gas and liquid) upon an increase in total superficial velocity. Both theory and laboratory data show that, for fixed foam quality, a plot of ∇p or μ_{app} as a function of total superficial velocity forms an S-shaped curve (Kam, 2008; see also Fig. 16 in Gauglitz et al. (2002)). The curve is reminiscent of catastrophe theory (Zeeman, 1977), also known as bifurcation theory. Figure 1a represents foam generation in terms of the response of total interstitial velocity v_t as a function

of ∇p . Three foam regimes are identified: lower, coarse-foam regime with low ∇p ; upper, strong-foam regime with high ∇p ; and intermediate foam regime with ∇p between the other two regimes. As stated in catastrophe theory, the intermediate regime is intrinsically unstable (no tolerance to perturbations in ∇p or v_t); this was observed experimentally by Gauglitz et al. (2002). This suggests that foam states in this regime cannot be observed naturally.

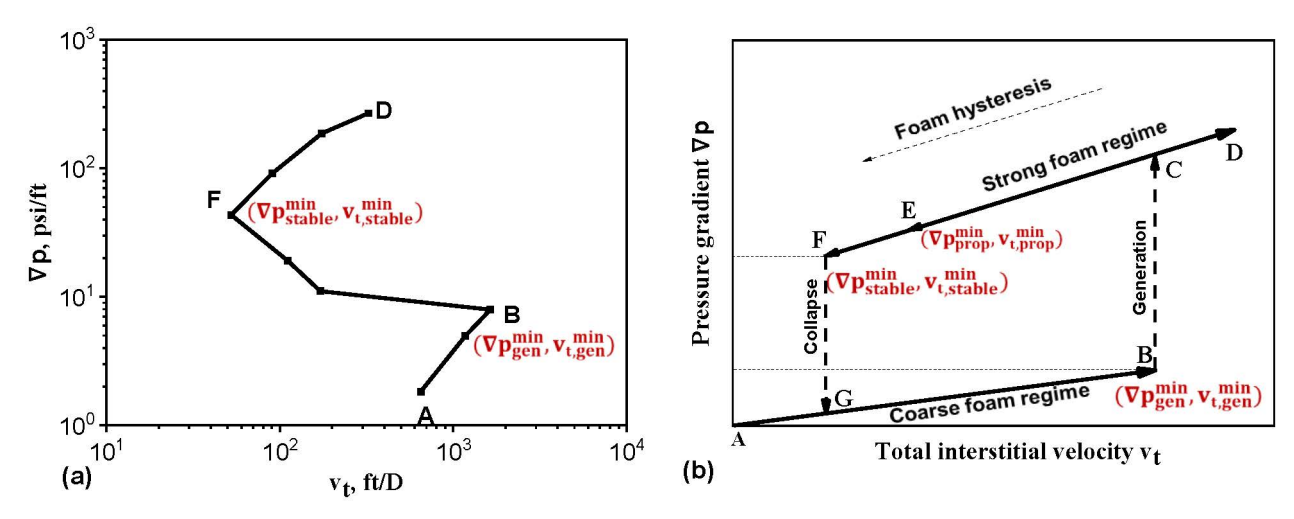


Figure 1—Foam generation as a function of pressure gradient, ∇p (left figure) or total interstitial velocity, vt (right figure): (a) vt as a function of ∇p in a sequence of increasing ∇p following A-B-F-D (Gauglitz et al., 2002), and (b) schematic of ∇p as a function of vt in a sequence of increasing, then decreasing, vt following A-B-C-D-E-F-G (Yu et al., 2020). The letter labels in Fig. 1a correspond to those in Fig. 1b. Fig. 1a is N₂ foam data in Boise sandstone of 7.1 Darcies, taken from Gauglitz et al. (2002).

The data in Fig. 1a were obtained by fixing ∇p across a core at a fixed u_w in steady-state corefloods, where gas rates were measured in each step of increased ∇p . In the observed unstable regime it was very difficult to maintain both fixed ∇p and foam quality. With increasing ∇p from point A to B, foam is coarse and gas velocity (u_g) has to increase to meet the preset ∇p in each step. Thereafter, foam enters the intermediate regime where the curve folds back towards lower velocities. This is because the population of lamellae increases with ∇p to an extent that gas-mobility reduction is more than the ∇p increase, meaning lower u_g is needed to maintain the fixed ∇p . Starting from point F, the curve folds forwards again, entering strong-foam regime with u_g increasing with ∇p .

In the literature, most studies examine foam generation by fixed injection rate, instead of fixed ∇p . In an experiment with fixed injection rate increasing in steps, foam generation is schematically illustrated in Fig. 1b in terms of the response of ∇p as a function of total interstitial velocity v_t . Given the unstable nature of the intermediate regime in Fig. 1a, ∇p makes an upward jump with increasing v_t , instead of folding back. The onset of the upward jump marks the minimum pressure gradient, ∇p_{gen}^{min} (point B), or an equivalent minimum total interstitial velocity, $v_{t,gen}^{min}$, for triggering strong foam. With sufficient decrease in v_t , ∇p makes an abrupt downward jump, meaning abrupt foam collapse. The onset of the downward jump indicates a minimum pressure gradient ∇p_{stable}^{min} (point F) or an equivalent minimum total interstitial velocity $v_{t,gen}^{min}$ for maintaining a stable foam (Yu et al., 2020).

The N₂ foam data of Yu et al. (2020) in a 2.5-Darcy Bentheimer sandstone also show the existence of a minimum pressure gradient and velocity for propagation, ∇p_{prop}^{min} and $v_{t,prop}^{min}$ (point E). Below this critical value, foam does not propagate, though it is maintained in place. The critical thresholds for foam generation, stability and propagation follow the relation: $\nabla p_{prop}^{min} > \nabla p_{stable}^{min} > > \nabla p_{gen}^{min}$, with $v_{t,gen}^{min} \gg v_{t,prop}^{min} > v_{t,stable}^{min}$. This suggests that foam propagation is more challenging than generation at low pressure gradient. The conditions for foam propagation depend on the same mechanisms as though for generation, however (Ashoori et al., 2012; Yu and Rossen, 2022).

Correlations between ∇p_{gen}^{min} and K

In the literature, several quantitative correlations between ∇p_{gen}^{min} and K have been reported. Most data obtained for fitting those correlations are with N_2 foam. For CO_2 foam, the quantitative correlations between ∇p_{gen}^{min} and influential factors are unclear, given the lack of data.

Based on a percolation theory of Rossen and Gauglitz (1990), Gauglitz et al. (2002) find that ∇p_{gen}^{min} scales with K as K⁻¹ for unconsolidated porous media:

$$\nabla p_{gen}^{\min} \sim K^{-1} \tag{1}$$

Equation 1 is based on the pressure difference over an individual liquid lens, incorporating the impact of pore geometry. This correlation is in good agreement with Gauglitz et al.'s N_2 foam data.

Ransohoff and Radke (1988) present a critical capillary number of 8 for generation, using the definition of

$$N_c = \frac{\mu_{nw} v_t \varphi L R_g}{\sigma K K_{rnw}} = \frac{\nabla p L R_g}{f_{nw} \sigma} \tag{2}$$

where μ_{nw} – viscosity of the nonwetting phase (gas here), v_t – total interstitial velocity, φ – medium porosity, L - medium length, R_g – rock grain radius, σ – surface tension, K – permeability and K_{rnw} – nonwetting-phase relative permeability, ∇p – pressure gradient across the medium, f_{nw} – nonwetting-phase fraction. Gauglitz et al. (2002) convert the left equation to the right one using Darcy's law for gas phase. Then, substituting N_{ca} = 8 into the right side of Eq. 2 converts the critical capillary number to ∇p_{gen}^{min} :

$$\nabla p_{gen}^{\min} = \frac{8f_{nv}\sigma}{L} \sqrt{\frac{4\varphi^3}{150K(1-\varphi)^2}} \tag{3}$$

 ∇p_{gen}^{min} converted from Ransohoff and Radke (1988) actually is related to capillary-entry pressure, not directly to the minimum pressure gradient required for generation (Rossen, 1996).

Tanzil et al. (2000; 2002) report another critical capillary number of 2 for generation, using the definition of

$$N_c = \frac{\Delta p}{\sigma} \sqrt{\frac{K}{\varpi}} = 2 \tag{4}$$

where the parameters here have the same definitions as in Eq. 2. Gauglitz et al. (2002) convert Eq. 4 to a minimum pressure gradient, through the Blake-Kozeny correlation for K (Bird et al., 2002):

$$\nabla p_{gen}^{\min} = \frac{2\sigma}{L} \sqrt{\frac{\varphi}{K}} \tag{5}$$

where L is the length of the medium. However, the experiments of Tanzil et al. (2000; Tanzil et al. 2002) were conducted in a drainage process, not steady-state.

Experimental Methodology

Figure 2 shows a schematic of the coreflood apparatus used in our study. The whole setup was placed in an oven except for the pumps and data-recording system. We used dual ISCO pumps to allow for continuous co-injection of gas and liquid that were stored in respective transfer vessels. A Hassler core holder was used and mounted vertically, with fluids injected from the top, to avoid gravity segregation. Two absolute pressure transducers of accuracy \pm 0.01 bars are used to measure overall pressure drops across a core. Pressure (P) in the system is controlled via a back-pressure regulator (BPR) of accuracy \pm 1 bar.

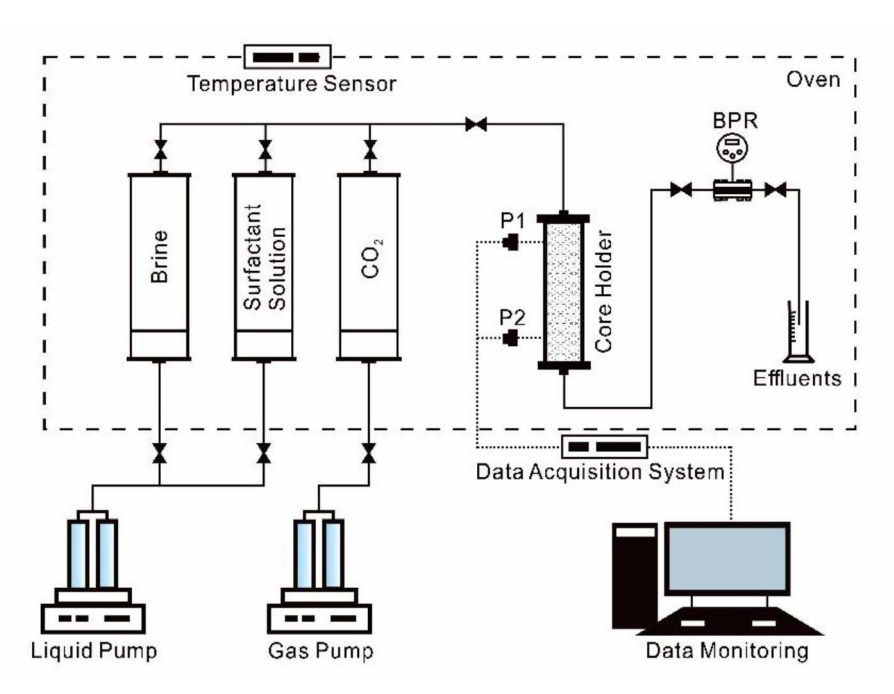


Figure 2—Schematic of the coreflood apparatus for foam-generation study at fixed injection flow rates.

The whole setup is placed inside an oven except for injection pumps and data-collection system.

For the purpose of the study, we examined permeabilities K in the range of $10 - 10^3$ mD, injected quality f_g from 0.5 - 0.9 and different surfactant concentrations C_s . All our experiments were conducted at 40° C with a back-pressure 80 bars, with CO_2 in the supercritical state. The quality f_g was fixed in each experiment and gas and liquid were injected following the v_t sequence as in Fig. 1b: increase v_t in steps through a few points after strong foam was observed and then reduce v_t to the initial value. ∇p was recorded with time for each v_t . To ensure steady state, at least 2 PV of surfactant solution was injected in each measurement.

Table 1 lists the experimental materials and properties of the rock and fluids. We use homogeneous artificial consolidated sandstone cores (Al Homadhi, 2002; Jishun, 2004; Wang et al., 2012) from Tiandi Science & Technology in Beijing, China. The relative-permeability functions for water and gas without foam are referred to those measured in homogeneous Bentheimer Sandstone (Eftekhari and Farajzadeh, 2017). The foaming agent examined was APG0814 (a nonionic surfactant with a carbon-chain length of C_8 – C_{14}) from Shanghai Acmec Biochemical in China. We also measured supercritical CO_2 -surfactant surface tension σ at different values of C_s , using a pendant-drop tensiometer, DSA100HP690, from KRÜSS Scientific in Hamburg, Germany.

Table 1—Rock and fluid properties at the experimental conditions $T = 40^{\circ}C$ and P = 80 bar.

Materials	Properties
Artificial consolidated	$\emptyset = 2.5 \text{ cm} \text{ and } L = 8 \text{ cm}$
	$K_1 = 27 \text{ mD}, \phi_1 = 0.17$
sandstone cores	$K_2 = 274 \text{ mD}, \phi_2 = 0.21$
	$K_3 = 905 \text{ mD}, \phi_3 = 0.24$
CO ₂	$\mu_g = 0.03 \ cp$
Brine, 3 wt% NaCl	$\mu_w = 0.7 \ cp$
Water relative permeability	$K_{rw}(S_w) = 0.713 \left(\frac{S_w - 0.135}{0.665}\right)^{2.46}$

Materials	Properties
Gas relative permeability without foam	$K_{rg}^{nf}(S_g) = 0.94 \left(\frac{S_g - 0.2}{0.665}\right)^{1.3}$
	σ = 2.82 mN/m at C_s = 1 wt%
	$\sigma = 2.87 \text{ mN/m at } C_s = 0.5 \text{ wt}\%$
	$\sigma = 2.96 \text{ mN/m} \text{ at } C_s = 0.1 \text{ wt}\%$
Surfactant APG0814*	$\sigma = 4.26 \text{ mN/m} \text{ at } C_s = 0.05 \text{ wt}\%$
	$\sigma = 10.70$ mN/m at $C_s = 0.01$ wt%
	σ = 12.91 mN/m at C_s = 0 wt%

^{*} σ was measured at T = 50°C and P = 80 bar

Experimental Results and Discussion

Determination of ∇p_{gen}^{min} **for** CO_2 **Foam**

Figure 3 shows our data for ∇p_{gen}^{min} at a fixed $f_g = 0.6$ in the 905-mD core. Arrows indicate the increasing-then-decreasing velocity sequence where ∇p is measured. All the experiments in our study follow the same v_t sequence.

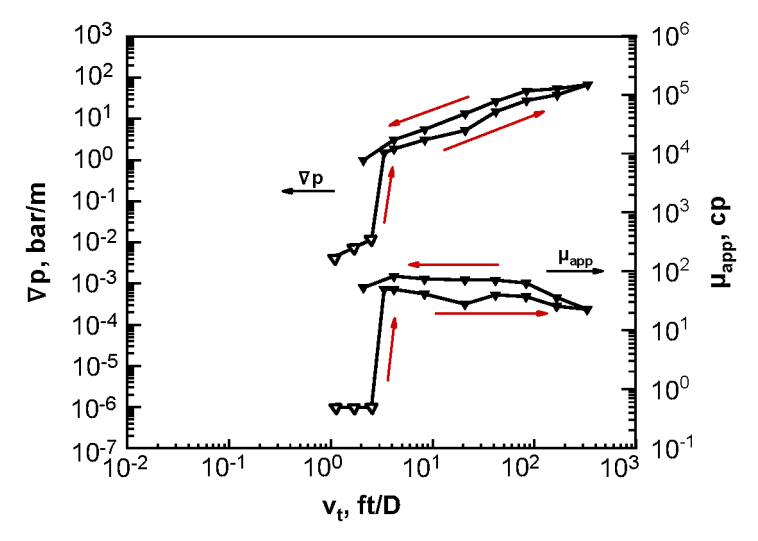


Figure 3—Pressure gradient ∇p (bar/m) and apparent viscosity μ_{app} (cp) as a function of total interstitial velocity v_t (ft/D) in the 905-mD core. Each symbol represents a steady-state measurement at a fixed quality $f_g = 0.6$; open symbols denote values estimated based on Darcy's law, as ∇p was too low to be measured for those points in our study. Arrows indicate the v_t sequence imposed.

In this case and some cases below, ∇p is too low to be measurable at low velocities in our experiments. Gauglitz et al. (2002) show that in a Boise core of 950 mD, ∇p for coarse CO_2 foam is almost the same as CO_2 -water injection without foam. So we estimate those ∇p values as denoted by the open symbols in Fig. 3. Based on Darcy's law for gas-liquid injection without foam, quality f_g is defined as

$$f_g = \frac{k_{rg}^{nf} / \mu_g}{k_{rw} / \mu_w + k_{rg}^{nf} / \mu_g} \tag{6}$$

Substituting the relative-permeability functions in Table 1 into Eq. 6, one can calculate gas and water saturations at $f_g = 0.6$. Then one can calculate the corresponding ∇p at a given vt without foam, based on total superficial velocity $(v_t \times \varphi)$.

At low v_t , ∇p is very low, reflecting few or no lamellae created, corresponding to the coarse-foam regime in Fig. 1. With increasing v_t at $v_{t,gen}^{min}$, ∇p , as seen from Fig. 3, jumps upward abruptly by two orders of magnitude, marking the onset of strong-foam generation. The value of ∇p estimated just before the jump approximates the $v_{t,gen}^{min}$ (point B in Fig. 1) for triggering strong foam. In Fig. 3, ∇p_{gen}^{min} is ~ 0.01 bar/m (~ 0.04 psi/ft), very easily attainable throughout the formation during foam injection. This value is about two orders of magnitude less than for N_2 foam, e.g. $\nabla p_{gen}^{min} \sim 4.52$ bar/m (20 psi/ft) at $f_g = 0.88$ in a 2.5-Darcy Bentheimer sandstone core (Yu et al., 2020). The considerable difference in ∇p_{gen}^{min} values demonstrates that foam generation deep in a formation, where ∇p is low, restricts the long-distance propagation of N_2 foam but is much less an issue for CO_2 foam.

The minimum total interstitial velocity $v_{t,gen}^{min}$ and pressure gradient ∇p_{gen}^{min} are related by Darcy's law:

$$v_{t,gen}^{\min} = \frac{1}{\varphi} K \lambda_{rt} \nabla p_{gen}^{\min} \tag{7}$$

where

$$\lambda_{rt} = \frac{k_{rw}}{\mu_w} + \frac{k_{rg}^f}{\mu_g} \tag{8}$$

where λ_{rt} is the total relative mobility and superscript in k_{rg}^f denotes the effective gas relative permeability with foam. Although we set injection rate and measure ∇p , ∇p_{gen}^{min} is the key for foam generation; $v_{t,gen}^{min}$ is the velocity needed to meet the required value of ∇p_{gen}^{min} . This is because the mechanisms of lamella creation occur in a mobilization process, driven by certain pressure gradient.

We also show foam apparent viscosity associated with the ∇p data, defined as

$$\mu_{app} \equiv \frac{1}{\lambda_{rt}} \tag{9}$$

Consistent with the ∇p response, apparent viscosity μ_{app} at ∇p_{gen}^{min} jumps abruptly from 0.49 to 49 cp and foam generation erupts everywhere along the core suddenly. This marks that foam enters the strong regime. In the decreasing- v_t sequence, foam strength (μ_{app}) is greater than in the increasing sequence, with a 40-80 % hysteresis in μ_{app} between the two v_t sequences. In addition, foam in the strong-foam regime appears to be shear-thinning for both increasing and decreasing v_t : μ_{app} falls by a factor ~ 2 over a 100-fold increase in v_t . Assuming $f_g = 0.6$ is in the low-quality strong-foam regime (Kim et al., 2005; Tang et al., 2019a), stability is not an issue there. The hysteresis and shear-thinning likely arise from fraction of the trapped bubbles varying with v_t .

At velocities below $v_{t,gen}^{min}$, strong foam can be maintained, with much lower mobility than coarse foam at the same velocity. Thus strong foam can be maintained at velocities lower than $v_{t,gen}^{min}$, but it requires a ∇p much greater than ∇p_{gen}^{min} to mobilize it. Since the velocities tested in the decreasing sequence were not low enough, we could not determine the exact value of ∇p_{gen}^{min} (point F in Fig. 1) for maintaining a stable foam. However, its value would be less than 1 bar/m, the last measured datum, which is 1 - 2 orders of magnitude less than N2 foam (Yu et al., 2020). One cannot determine the minimum ∇p for strong-foam propagation, ∇p_{gen}^{min} (point E in Fig. 1) from the data as in Fig. 3 obtained in a straight core. The N₂ foam data of Yu et al. (2020) from a variable-diameter core show that its value is greater than ∇p_{stable}^{min} and much greater than ∇p_{gen}^{min} . For CO₂ foam, more research is needed to quantify ∇p_{stable}^{min} and ∇p_{prop}^{min} .

Effect of Injected Quality

The percolation theory of Rossen and Gauglitz (1990) predicts that foam generation shows a dependence on f_g . Their data and those in Kam and Rossen (2002) and Yu et al. (2020) experimentally validate this dependence for N_2 foam. Here we show the effect of f_g on CO_2 foam generation and quantify the correlations between $\left(\nabla p_{gen}^{min} v_{t,gen}^{min}\right)$ and f_g .

We measured ∇p_{gen}^{min} as a function of injected quality f_g in cores of permeabilities 905, 274 and 27 mD. Field selection of injected f_g depends on chemical cost (amount of surfactant injected) and effectiveness of mobility control by strong foam. An optimal injection strategy would be choosing a value f_g in the low-quality strong-foam regime close to the transition foam quality fg^* ($\sim 0.7 - 0.9$), at which mobility reduction is at its maximum (Alvarez et al., 2001). This would maximize the potential of mobility control while minimizing the amount of surfactant injected. Here we examine f_g above 0.5.

Figure 4 displays the ∇p_{gen}^{min} measurements for f_g ranging from 0. 5 to 0.9 in the 905-mD core. The value of ∇p before foam generation could not be measured, as indicated by the open symbols; it is estimated from v_t based on Darcy's law. The data suggest ∇p_{gen}^{min} rising with increasing f_g by a factor about 4, within the order of 10^{-3} to 10^{-2} bar/m. ∇p in the field could easily go beyond such low ∇p_{gen}^{min} . The equivalent $v_{t,gen}^{min}$ values also increase with f_g but by a factor about 10. As seen from Eq. 7, the difference reflects greater λ_{rt} with increasing f_g (Eq. 8), at the onset of strong foam generation.

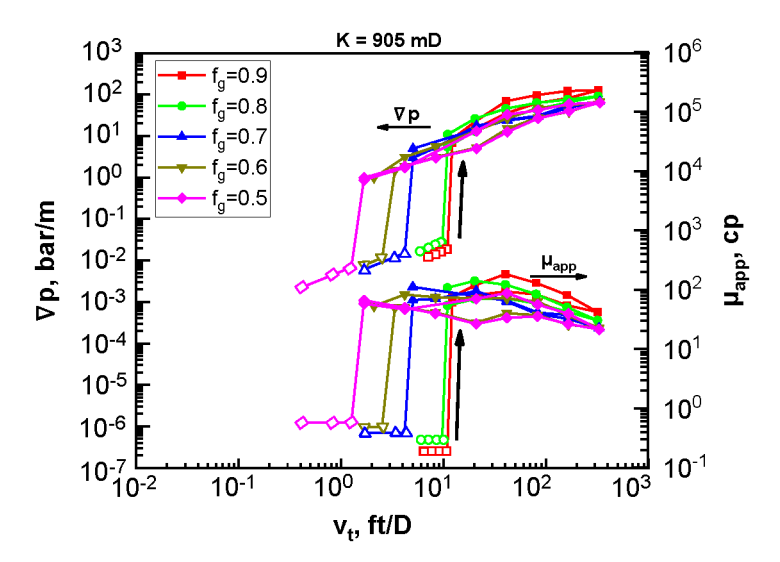


Figure 4—Pressure gradient ∇p (bar/m) and apparent viscosity µ_{app} (cp) as a function of total interstitial velocity, v_t (ft/D), in the core of 905 mD, with various injected qualities f_g. Each curve represents steady-state measurements at a fixed f_g with v_t in an increasing-then-decreasing sequence as in Fig. 1b. Open symbols indicate points estimated from Darcy's law as described in the previous section.

In most cases in Fig. 4, the strong foam exhibits up to a 150 % increase in ∇p and μ_{app} in the decreasing v_t sequence compared to the increasing sequence; the hysteresis is stronger at wet conditions (low f_g). Also, the strong-foam data show shear-thinning behvior, with μ_{app} reduced by 1.5 – 3 times over 100-fold increase in v_t .

The theory of Rossen and Gauglitz (1990) also predicts that ∇p required for mobilization of the strong foam is lower at wet conditions. The prediction is supported in Fig. 4; ∇p shows a 3 – 5-fold decrease, with decreasing f_g .

Figure 5 presents the ∇p_{gen}^{min} measurements v. f_g in the 274-mD core. ∇p_{gen}^{min} and equivalent $v_{t,gen}^{min}$ each again shows a positive correlation with f_g . The values of ∇p_{gen}^{min} fall within the range from 10^{-2} to 10^{-1} bar/m (~

0.04-0.44 psi/ft), one order of magnitude greater than in Fig. 4 in the 905-mD core. The values of $v_{t,gen}^{min}$ are also greater than in Fig. 4 and increase by a factor ~ 15 over the f_g range 0.5 - 0.9. This suggests that foam generation is more difficult in low-permeability media, whereas the low range of ∇p_{gen}^{min} (< 1 psi/ft) does not restrict the generation deep in formations.

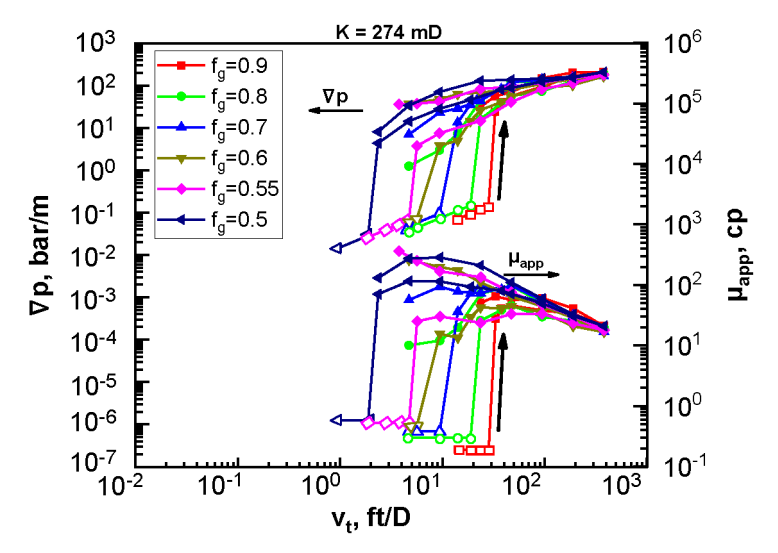


Figure 5— ∇p (bar/m) and μ_{app} (cp) as a function of v_t (ft/D) in the core of 274 mD, with respect to fixed injected f_g . Each curve represents steady-state measurements at a fixed f_g with v_t increasing-then-decreasing in a sequence as in Fig. 1b. Open symbols indicate data points estimated from Darcy's law using relative-permeability functions in Table 1.

As in Fig. 4, strong foam exhibits similar hysteresis (50 - 150 % in most cases) and shear-thinning (μ_{app} reduced by 1.5 - 5 times). Nevertheless, unlike the monotonic dependence in Fig. 4, ∇p in the strong-foam regime, in general, increases with f_g and then decreases. This could reflect the two flow regimes of strong foam (Kim et al., 2005; Tang et al., 2019a), where ∇p increases with f_g in the low-quality regime until a transition quality f_{g^*} and then decreases with f_g in the high-quality regime. Foam in a high-K medium is more stable and often has a greater f_{g^*} (Kapetas et al., 2017). In Fig. 4, the f_g values where ∇p upon foam generation increases with f_g are likely less than f_{g^*} , residing in the low-quality regime, while the values where ∇p decreases with f_g are in the high-quality regime.

In the core of 27 mD (Fig. 6), ∇p_{gen}^{min} shows a similar increasing trend with f_g as in Figs. 4 and 5. The values of ∇p_{gen}^{min} are much greater than in Figs. 4 and 5, lying within the range of 5 - 15 bar/m (~ 15 - 66 psi/ft). Though this range is lower than for N₂ foam, it is still a challenge to attain such high ∇p_{gen}^{min} deep in a formation. Factors such as formation heterogeneity and alternating slug injection of gas and liquid may reduce ∇p_{gen}^{min} facilitating foam generation in low-K reservoirs, allowing for deep foam generation (Rossen, 1999; Bertin et al., 1999; Li and Rossen, 2005; Fernø et al., 2016; Skauge et al., 2020). In this case, the curves in the strong-foam regime nearly overlap and exhibit strongly shear-thinning behavior.

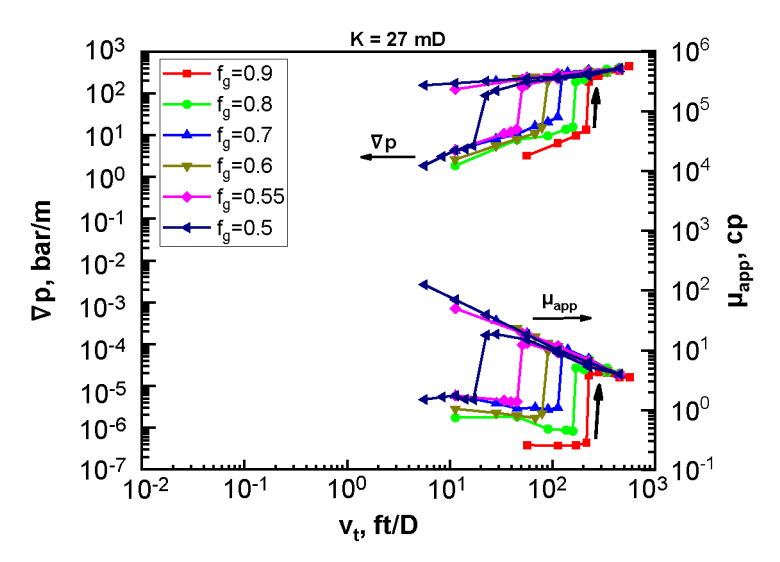


Figure 6— ∇p (bar/m) and μ_{app} (cp) as a function of v_t (ft/D) in the core of 27 mD, with various injected f_g . In this and subsequent plots, each curve represents steady-state measurements at a fixed f_g with v_t in an increasing-then-decreasing sequence as in Fig. 1b.

Correlations between $(\nabla p_{gen}^{min}, v_{t,gen}^{min})$ and f_g . Fig. 7 plots $(\nabla p_{gen}^{min}, v_{t,gen}^{min})$ as a function of f_g from Figs. 4 - 6 and a linear fitt to the data on log-log scale. The slopes do not vary significantly with respect to K: 1.1, 2.5 and 2.1 in Fig. 7a and 3.9, 4.3 and 3.9 in Fig. 7b for 27, 274 and 905 mD, respectively. This indicates that K has a mild impact on the correlation of ∇p_{gen}^{min} v. f_g and of $v_{t,gen}^{min}$ v. f_g .

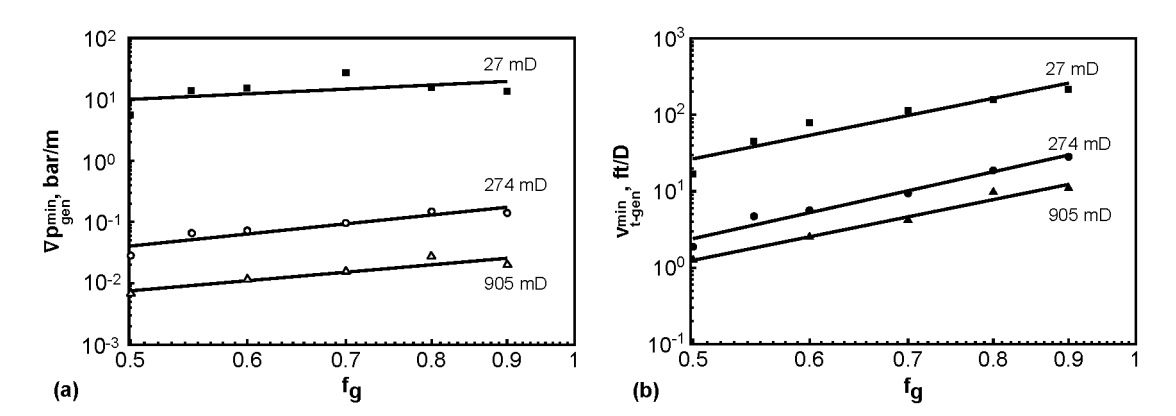


Figure 7—(a) Minimum pressure gradient ∇p_{gen}^{min} and (b) minimum total interstitial velocity $v_{t,gen}^{min}$ for CO_2 foam generation as a function of foam quality f_g . The data here for $(\nabla p_{gen}^{min}, v_{t,gen}^{min})$ are taken from Figs. 4–6, i.e. values of ∇p and v_t observed right before the ∇p jump, corresponding to point B in Fig. 1b.

One can then approximate, based on average of the slopes, that ∇p_{gen}^{min} scales with f_g approximately as $(f_g)^2$ for K ranging 20 - 1000 mD:

$$\nabla p_{gen}^{\min} \sim \left(f_g \right)^2 \tag{10}$$

Similarly, $v_{t,gen}^{min}$ approximately scales with f_g as $(f_g)^4$ for K = 20 - 1000 mD:

$$v_{t,gen}^{\min} \sim \left(f_g\right)^4 \tag{11}$$

Moreover, the values of $v_{t,gen}^{min}$ for 27 mD are about 20 times greater than for 905 mD for all tested values of f_g , while the permeability ratio is 33. Gauglitz et al. (2002) found that ∇p_{gen}^{min} scales as (1/K) for unconsolidated sand and bead packs, which suggests that $v_{t,gen}^{min}$ is nearly independent of K.

Given that not many data points are available, the correlations in Eqs. 10 and 11 reflect some uncertainty. More data are needed to improve the confidence of these correlations.

Effect of Surfactant Concentration

Surfactant type and concentration (C_s) play a significant role in foam generation, as the accumulation of lamellae depends on the stability of lamellae created. For concentrations below the critical micelle concentration (CMC), the dependence of lamella stability on C_s is especially severe. Moreover, below the CMC surfactant concentration affects surface tension and thereby the ease of mobilizing lamellae. The surfactant concentration deployed in the field is often relatively low (though far greater than the CMC) given the chemical cost. Moreover, deep in formations, C_s is subject to adsorption by rock and dilution by formation water. Here we show how C_s affects foam generation at low concentrations, for low- and high-quality injection, respectively.

Figure 8 plots ∇p_{gen}^{min} measurements with respect to C_s , for low-quality injection in the 27-mD core. Throughout these measurements, injected quality f_g is fixed at 0.5, chosen such that the strong foam generated resides in the low-quality regime. The surfactant used here has a CMC \sim 0.05 wt% at room pressure and temperature, and the C_s ranges from 0.01 to 0.5 wt% in these experiments.

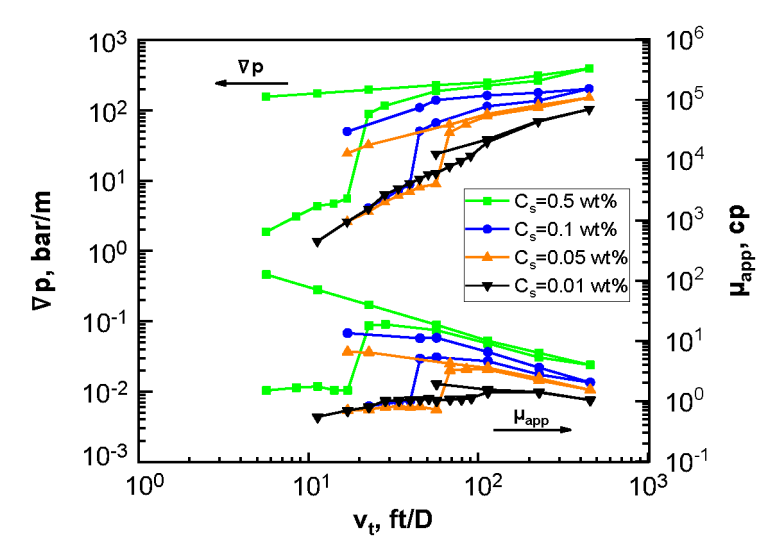


Figure 8— ∇p (bar/m) and μ_{app} (cp) as a function of v_t (ft/D) in the 27-mD core, with respect to surfactant concentration C_s : low-quality foam injection. For all C_s examined, the injected quality was fixed at f_q = 0.5.

As in Figs. 4 - 6, ∇p jumps abruptly when strong foam is triggered, and the magnitude of the jump is greater at higher C_s . For $C_s \ge CMC$, as one expects, ∇p_{gen}^{min} and $v_{t,gen}^{min}$ show an increasing trend with decreasing C_s . The impact of C_s on ∇p_{gen}^{min} above the CMC, however, is mild; ∇p_{gen}^{min} increases by a factor less than 2 and $v_{t,gen}^{min}$ by a factor ~ 3 , for a 10-fold reduction in C_s from 0.5 to 0.05 wt%.

For the case of $C_s = 0.01$ wt% < CMC (black curve in Fig. 8), ∇p shows a continuous, though steep, increase with increasing v_t , instead of a jump as indicated in Fig. 1b. Similar behavior was reported by Kibodeaux (1997). The μ_{app} values reflect the presence of very-coarse foam, e.g., 1 - 1.5 cp greater than 0.58 cp estimated from Darcy's law for no foam.

Figure 9 shows ∇p_{gen}^{min} at various C_s for f_g fixed at 0.9. With high-quality injection, foam generation is more sensitive to C_s . For $f_g = 0.9$ in Fig. 9, ∇p_{gen}^{min} rises threefold over a fivefold reduction in C_s , compared to twofold over a tenfold reduction in C_s at $f_g = 0.5$ in Fig. 8. Also, the trigger for strong foam requires a higher C_s for high quality, as seen from the ∇p jump that occurs with $C_s \ge 0.1$ wt% for $f_g = 0.9$ in Fig. 9, compared to $C_s \ge 0.05$ wt% for $f_g = 0.5$ in Fig. 8. This suggests that a minimum surfactant concentration may be needed to trigger strong foam, and the higher the f_g , the greater the required concentration would be. In the cases where no strong foam is triggered as in Fig. 1b, foam at very low values of C_s still maintains some strength in the decreasing v_t sequence.

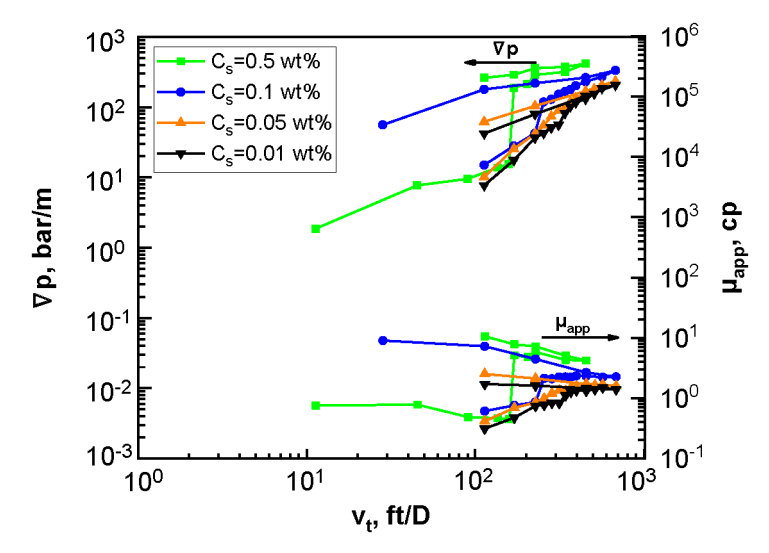


Figure 9— ∇p (bar/m) and μ_{app} (cp) as a function of v_t (ft/D) in the 27-mD core, with respect to surfactant concentration C_s : high-quality foam injection. For all C_s examined, the injected quality was fixed at f_q = 0.9.

Correlations between $(\nabla p_{gen}^{min}, v_{t,gen}^{min})$ and C_s . Figure 10 plots ∇p_{gen}^{min} and $v_{t,gen}^{min}$ against C_s , respectively. The data in Fig. 10 are taken from Figs. 8 and 9. Solid lines represent linear fitting to the data on log-log scale. The slopes of the linear lines do not change greatly between $f_g = 0.5 - 0.9$. Based on average of the slopes, one can get an approximate correlation for ∇p_{gen}^{min} v. C_s :

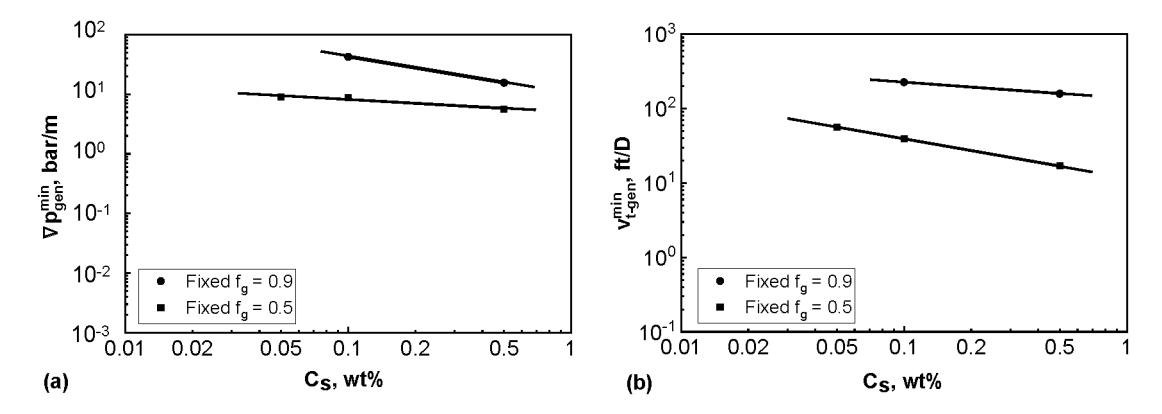


Figure 10—(a) Minimum pressure gradient ∇p_{gen}^{min} and (b) minimum total interstitial velocity $v_{t,gen}^{min}$ for CO_2 foam generation as a function of surfactant concentration C_s . The data here for $\left(\nabla p_{gen}^{min}, v_{t,gen}^{min}\right)$ are values of Vp and v_t observed right before the ∇p jump in Figs. 7–8, corresponding to point B in Fig. 1b.

$$\nabla p_{gen}^{\min} \sim \left(C_s\right)^{-0.4} \tag{12}$$

where the slope in Fig. 10a is ~ 0.2 at $f_g = 0.5$ and ~ 0.6 at $f_g = 0.9$. Similarly, one can estimate the correlation for $v_{t,gen}^{min}$ v. C_s as

$$v_{t,gen}^{\min} \sim \left(C_s\right)^{-0.4} \tag{13}$$

where the slope in Fig. 10b is ~ 0.5 at $f_g = 0.5$ and ~ 0.2 at $f_g = 0.9$.

However, given that the data available are very limited, the powers in Eqs. 12 and 13 are uncertain. More data are needed to verify or improve the accuracy of the correlations.

Effect of Permeability: Comparison between CO₂ and N₂ Foams

Figure 11 compares the ∇p_{gen}^{min} data as a function of K between CO_2 (filled symbols) and N_2 (open symbols) foams, respectively. The CO_2 data are from this study in artificial consolidated sandstone cores and the N_2 data are from Gauglitz et al. (2002) mostly in sand/bead packs, with some data from outcrop rock cores. The solid lines represent a linear fit to the data in each case on log-log scale. For our CO_2 foam data, there is some variation depending on injected quality f_g . The differences in porous media complicate the comparison between N_2 and CO_2 .

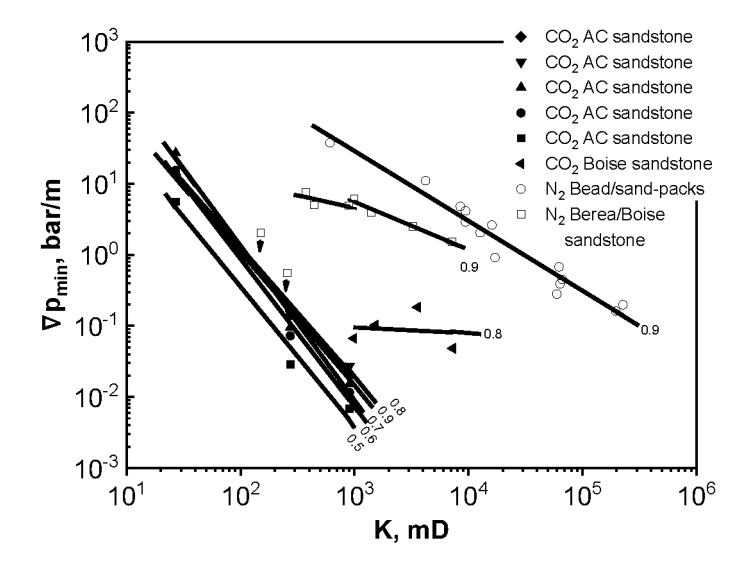


Figure 11—Comparison of ∇p_{gen}^{min} as a function of permeability K between CO₂ and N₂ foam. AC in the legend denotes artificial consolidated sandstone, and filled symbols represent the data for CO₂ and open symbols for N₂. Solid lines are linear fit to the data and numbers labelled indicate the injected quality f_g in each case. The CO₂ foam data in Boise sandstone and all the N₂ foam data are taken from Gauglitz et al. (2002).

The values of ∇p_{gen}^{min} for CO_2 foam are 2-3 orders of magnitude less than for N_2 foam in the K range examined. The lower ∇p_{gen}^{min} for CO_2 partly arises from lower surface tension for CO_2 -surfactant than N_2 -surfactant (Farajzadeh et al., 2009). This suggests that longdistance propagation deep in formations with limited ∇p is much less an issue for CO_2 foam than for N_2 foam.

The N₂ data in homogeneous bead/sand packs (upper right in Fig. 11) are in good agreement with the correlation in Eq. 1, showing that ∇p_{gen}^{min} scales as K_{-1} . The CO₂ data (lower left in Fig. 11) show, however, that ∇p_{gen}^{min} scales with K as K^{-2} in consolidated sandstone:

$$\nabla p_{gen}^{\min} \sim K^{-2} \tag{14}$$

The correlations in Eqs. 1 and 14 differ, primarily because the correlations between ∇p_{gen}^{min} pore geometry and K are more complex in consolidated media than assumed in the theory of Rossen and Gauglitz (1990).

For CO₂ foam in the Boise sandstone, ∇p_{gen}^{min} is nearly independent of K, instead of scaling as a power function of K, though Gauglitz et al. (2002) report substantial uncertainty in the data. One likely explanation could be that Boise sandstone is not ideally homogeneous and helps foam generation by heterogeneity. This also suggests that in addition to sharp permeability boundaries as reported by Shah et al. (2019), local permeability heterogeneity may also significantly help foam generation. The heterogeneity in K is associated with heterogeneity in capillarity, which would cause capillary-pressure fluctuations and help lamella creation. Further research is needed to demonstrate whether ∇p_{gen}^{min} is truly independent of K in heterogeneous rocks.

Conclusions

In steady injection (i.e., not drainage), CO₂ foam exhibits a critical threshold in pressure gradient, ∇p_{gen}^{min} or total interstitial velocity, $v_{t,gen}^{min}$ beyond which strong-foam generation is triggered from a state of coarse or no-foam.

The effects of factors on ∇p_{gen}^{min} and $v_{t,gen}^{min}$ have been determined, including injected quality (f_g) , surfactant concentration (C_s) and permeability (K). Conditions that stabilize lamellae reduce ∇p_{gen}^{min} and $v_{t,gen}^{min}$. Thus, ∇p_{gen}^{min} and $v_{t,gen}^{min}$ increase with increasing f_g , decrease with increasing f_g , and decrease with increasing f_g . We find the following correlations of f_g with f_g and f_g are f_g and f_g and f_g and f_g and f_g are f_g and f_g and f_g are f_g and f_g are f_g and f_g are f_g and f_g are f_g are f_g are f_g are f_g and f_g are f_g are f_g are f_g and f_g are f_g are f_g are f_g and f_g are f_g are f_g and f_g are f_g are f_g are f_g are f_g and f_g are f_g are f_g are f_g are f_g and f_g are f_g and f_g are f_g

- ∇p_{gen}^{min} scales with injected f_g as $(f_g)^2$; $v_{t,gen}^{min}$ scales with f_g as $(f_g)^4$.
- Both ∇p_{gen}^{min} and $v_{t,gen}^{min}$ scale with C_s as $(C_s)^{-0.4}$.
- ∇p_{gen}^{min} scales with K as K^{-2} , in comparison to K^{-1} for N_2 foam.

These correlations may be subject to uncertainty, and more data are needed to verify the confidence of these correlations.

For very low C_s , foam generation does not show an abrupt jump but shows, instead, a continuous, though steep, increase in upon increasing v_t . Thus, a minimum C_s , e.g., the CMC, may be needed to trigger strongfoam generation deep in a formation.

 ∇p_{gen}^{min} in the cores with K = 274 mD or greater is less than 0.17 bar/m (≤ 0.75 psi/ft), i.e. 2 - 3 orders of magnitude less than for N_2 foam. Such low ∇p_{gen}^{min} can be easily obtained in formations. This suggests that long-distance propagation for CO_2 foam is much less an issue for CO_2 foam than for N_2 foam.

 ${
m CO_2}$ foam propagation could be challenging in low-permeability homogeneous media; we find $\nabla p_{gen}^{min} \sim 10 \, {
m bar/m}$ for $K=27 \, {
m mD}$. However, formation heterogeneity and surfactant-alternating-gas injection strategy help foam generation. More research is needed to predict conditions for foam propagation under those conditions.

The propagation of foam requires a pressure gradient much greater than ∇p_{gen}^{min} for generation (Yu et al., 2020). More research is needed to quantify the minimum pressure gradient that allows foam to propagate into deep formation.

Acknowledgement

This project is funded by the UAEU Research Grant (Grant No.: 12N099) and partly by Open Fund of the State Key Lab of Oil and Gas Reservoir Geology and Exploration at SWPU (Grant No.: PLN2022-01).

References

Alvarez, J. M., Rivas, H. J., & W.R. Rossen. (2001). Unified model for steady-state foam behavior at high and low foam qualities. *SPE Journal*, **6**(03): 325–333.

- Al Homadhi, E. S. (2002). Artificial sandstone cores production with a wide range of petrophysical properties. *Journal of King Saud University Engineering Sciences*, **141**: 95–100.
- Ashoori, E., Marchesin, D., & Rossen, W.R. (2012). Multiple foam states and long-distance foam propagation in porous media. *SPE Journal* **17**(04): 1231–45.
- AlYousef, Z. A., Almobarky, M. A., & Schechter, D. S. (2018). The effect of nanoparticle aggregation on surfactant foam stability. *Journal of colloid and interface science*, **511**: 365–373.
- Bertin, H. J., Apaydin, O. G., Castanier, L. M., & Kovscek, A. R. (1999). Foam flow in heterogeneous porous media: effect of cross flow. *SPE Journal*, 4(02): 75–82.
- Bird, R. B., Stewart, W. E., & Lightfoot, E. N. (2002). Transport phenomena (2nd ed.). New York: Wiley.
- Bello, A., Ivanova, A., & Cheremisin, A. (2022). Enhancing N2 and CO2 foam stability by surfactants and nanoparticles at high temperature and various salinities. *Journal of Petroleum Science and Engineering*, **215**: 110720.
- Eftekhari, A. A., & Farajzadeh, R. (2017). Effect of foam on liquid phase mobility in porous media. *Scientific Reports* 7(March): 43870.
- Farajzadeh, R., Andrianov, A., Bruining, H., & Zitha, P.L. (2009). Comparative stiidy of CO2 and N2 foams in porous media at low and high pressure-temperatures. In *Industrial& Engineering Chemistry Research*, **48**(9): 4542–4552.
- Farajzadeh, R., Andrianov, A., Krastev, R., Hirasaki, G. J., & Rossen, W. R. (2012). Foamoil interaction in porous media: implications for foam assisted enhanced oil recovery. *Advances in Colloid and Interface Science*, **183-184**: 1–13.
- Fernø, M. A., Gauteplass, J., Pancharoen, M., Haugen, A., Graue, A., Kovscek, A. R., & Hirasaki, G. (2016). Experimental study of foam generation, sweep efficiency, and flow in a fractirre netivork. *SPEjournal*, **21**(04): 1140–1150.
- Gauglitz, P. A., Friedmann, F., Kam, S. I., & Rossen, W.R. (2002). Foam generation in homogeneous porous media, *Chemical Engineering Science*, **57**: 4037–4052.
- Jishun, Q. (2004). The manufacture and use of artificial consolidated core samples in China, Research Institute of Petroleum Exploration and Development, PetroChina. International Symposium of the Society of Core Analysts, Abu Dhabi, UAE, 5-9 October, 2004.
- Khatib, Z.R., Hirasaki, G.J., & Falls, A.H. (1988). Effects of capillary pressure on coalescence and phase mobilities in foams flowing through porous media, *SPE Journal* **3**(3): 919–926.
- Kibodeaux, K. (1997). Experimental and theoretical studies of foam mechanisms in enhanced oil recovery and matrix acidization applications. Ph.D. dissertation, University of Texas at Austin.
- Kam, S. I., & Rossen, W. R. (2002). A model for foam generation in homogeneous media. In Paper presented at the SPE Annual Technical Conference and Exhibition, San Antonio, Texas, September 2002.
- Kim, J. S., Dong, Y., & Rossen, W. R. (2005). Steady-state flow behavior of CO2 foam. SPE Journal, 10(04): 405–415.
- Kam, S. I. (2008). Improved mechanistic foam simulation with foam catastrophe theory. *Colloids and Surfaces A: Physicochemical and Engineering Aspects*, **318**(1-3): 62–77.
- Kapetas, L., Vincent-Bonnieu, S., Farajzadeh, R., Eftekhari, A. A., Mohd-Shafian, S. R., Bahrim, R. K., & Rossen, W. R. (2017). Effect of permeability on foam-model parameters: An integrated approach from coreflood experiments through to foam diversion calculations. *Colloids and Surfaces A: Physicochemical and Engineering Aspects*, **530**: 172–180.
- Li, Q., & Rossen, W. R. (2005). Injection strategies for foam generation in homogeneous and layered porous media. In Paper presented at the SPE Annual Technical Conference and Exhibition, Dallas, Texas, October 2005.
- Ransohoff, T. C., & Radke, C. J. (1988). Mechanisms of foam generation in glass-bead packs. In Society of Petroleum Engineers and Research Engineers, *SPE Reservoir Engineering*, 573–585.
- Rossen, W. R., & Gauglitz, P. A. (1990). Percolation theory of creation and mobilization of foams in porous media. *AIChE Journal*, **36**(8): 1176–1188.
- Rossen, W. R., & Zhou, Z. H. (1995). Modeling foam mobility at the "limiting capillary pressure". *SPE Advanced Technology Series* **3**: 146–153.
- Rossen, W.R. 1996. Foams in enhanced oil recovery, in R. K. Prud'homme and S. Khan, ed., *Foams: Theory, measurements and applications*, Marcel Dekker, New York, pp. 413–464.
- Rossen, W. R. 1999. Foam generation at layer boundaries in porous media. SPE Journal, 4(4): 409-412.
- Rossen, W. R. (2003). A critical review of Roof snap-off as a mechanism of steady-state foam generation in homogeneous porous media. *Colloids and Surfaces A: Physicochemical and Engineering Aspects*, **225**(1-3): 1–24.
- Rognmo, A. U., Heldal, S., & Fernø, M. A. (2018). Silica nanoparticles to stabilize CO2-foam for improved CO2 utilization: Enhanced CO2 storage and oil recovery from mature oil reservoirs. *Fuel*, **216**: 621–626.
- Rossen, W. R., Farajzadeh, R., Hirasaki, G. J., & Amirmoshiri, M. (2022). Potential and challenges of foam-assisted CO2 sequestration. In Paper presented at the SPE Improved Oil Recovery Conference, Virtual, April 2022.

Shah, S. Y., Wolf, K. H., Pilus, R. M., & Rossen, W. R. (2019). Foam generation by capillary snap-off in flow across a sharp permeability transition. *SPE Journal*, **24**(01): 116–128.

- Skauge, A., Solbakken, J., Ormehaug, P. A., & Aarra, M. G. (2020). Foam generation, propagation and stability in porous medium. *Transport in Porous Media*, **131**(1): 5–21.
- Tanzil, D. Hirasaki, G.J., & Miller, C.A. (2000). Mobility of foam in heterogeneous media: Flow parallel and perpendicular to stratification. SPE/DOE improved oil recovery symposium, Tulsa, OK, SPE 63228.
- Tanzil, D., Hirasaki, G. J., & Miller, C. A. (2002). Conditions for foam generation in homogeneous porous media. SPE/DOE improved oil recovery symposium, Tulsa, OK, SPE 75176.
- Tang, J., Vincent-Bonnieu, S., & Rossen, W. R. (2019a). Experimental investigation of the effect of oil on steady-state foam flow in porous media. *SPE Journal*, **24**(01): 140–157.
- Tang, J., Vincent-Bonnieu, S., & Rossen, W. R. (2019b). CT coreflood study of foam flow for enhanced oil recovery: The effect of oil type and saturation. *Energy*, **188**: 116022.
- Wang, H., Liu, Y., Song, Y., Zhao, Y., Zhao, J., & Wang, D. (2012). Fractal analysis and its impact factors on pore structure of artificial cores based on the images obtained using magnetic resonance imaging. *Journal of Applied Geophysics*, **86**: 70–81.
- Yu, G., Vincent-Bonnieu, S., & Rossen, W. R. (2020). Foam propagation at low superficial velocity: implications for long-distance foam propagation. *SPE Journal*, **25**(06): 3457–3471.
- Yu, G., and Rossen, W. R. (2022). Simulation models for the minimum velocity for foam generation and propagation. *Journal of Petroleum Science and Engineering*, **214**: 110406.
- Yu, W., Lo, J. H. Y., & Kanj, M. Y. (2023). Characterizing aqueous foams by in situ viscosity measurement in a foam column. *Langmuir*, **39**(41): 14711–14717.
- Zeeman, E. C. (1977). Catastrophe theory: selected papers (pp. 1972–1977). Boston: Addison-Wesley.